Bulletin of the
Seismological Society of America

Vol. 71 February 1981 No. 1

SOURCE INVERSION OF SEISMIC WAVEFORMS: THE KOYNA, INDIA, EARTHQUAKES OF 13 SEPTEMBER 1967

By Charles A. Langston

ABSTRACT

The treatment of the seismic source inverse problem, when diverse forms of waveform data are available, is simple and elegant using a moment tensor formalism. If earth structure is known and its effects predictable in terms of vertically inhomogeneous elastic-layered models, then all types of wave phenomena (e.g., surface waves, body waves, leaky modes, etc.) for a purely deviatoric moment tensor point source may be represented by, at most, a sum of three Green's functions. For an arbitrary symmetric moment tensor point source, one additional Green's function is needed for the *P-SV* system. However elegant this formalism may be for posing the linear inverse problem, the major difficulties lie in earth structure unknowns and resultant nonlinearities in the Green's functions which can cause significant trade-offs with source parameters. A hybrid inversion procedure is set up to gain insight into the probable unknowns in particular problems by incorporating both a linearized least-squares gradient method for the moment tensor or double couple, and smoothed time function parameters, and a nonlinear systematic trial-and-error search for moment tensor or double couple parameters for several assumptions of Green's function. The inversion technique is applied to near-regional waveform data from a small earthquake associated with the Koyna Reservoir which occurred 13 September 1967, as the second in a group of three events with very similar waveshapes, but differing amplitudes. The magnitudes of the second and third events are smaller by −0.2 and −0.8 units, respectively, compared to the first. The absolute magnitude for the first event is poorly constrained but is estimated to be 4.0 to 4.5 rather than the previously published value of 5.5 to 6.0. From the similarity of waveshapes, all three events are inferred to have the same mechanism and occurred within about 2 km of the same hypocenter. The results from moment tensor and double couple inversions for event 2 data indicate that source depth was 5 km and that left-lateral faulting occurred on a plane with a strike of N20°E ± 5°, dip of 90° ± 15°, and a rake of 0° ± 35°. The inferred far-field time function is approximately 3 sec in duration, unusually long for the seismic moment of 9×10^{22} dyne-cm, yielding a possible stress drop of about 0.05 bars. A fault map was constructed from LANDSAT image interpretation and shows a predominance of NNW to NNE striking faults in the Koyna area which is used to infer the appropriate nodal plane in the inversion results. These faults tend to define a broad en-echelon zone which parallels the Western Ghats in this area.

Introduction

The shaping of seismic waveforms involves a complex interaction of the seismic source with earth structure. If earth structure is adequately known, this complex interaction can be used to advantage to deduce source properties such as depth,

explosion yields, or fault orientation and time function. However, this is precisely the major problem with nearly all attempts to define seismic sources; knowledge of earth structure is always limited at some level of detail. For some data sets, such as long-period body waves, gross earth structure is sufficiently well known from other geophysical studies to place meaningful constraints on source properties (e.g., Burdick and Mellman, 1976). Other data are less suited to analysis because of unpredictable multipathing effects or simply because earth structure, elastic or otherwise, is not well resolved for the particular frequency band. An example of this is short-period *Lg* propagation at regional distances.

A major purpose of this paper is to extend and further develop inversion methods based on generalized ray techniques for dislocation sources used for teleseismic body waves to waveforms recorded at any distance (Helmberger, 1974; Langston and Helmberger, 1975; Burdick and Mellman, 1976; Langston, 1976, 1979). These may include body waves or surface waves of any type with the restriction that the structure be plane layered and, of course, known. A simple systematic search and test technique for orientation parameters is proposed on the basis of the form of the equations for the response due to an arbitrarily oriented point shear dislocation in a layered medium. Using the well-known result that an arbitrary oriented point shear dislocation is the sum of a vertical strike-slip, vertical dip-slip, and 45°-dipping dip-slip source, it becomes a straightforward matter to evaluate the structure response for each term and to model an observed waveform by summing the three solutions with the correct weighting factors. The weighting factors are, in turn, related to strike, dip, and rake. The search and test procedure (hereafter called the grid method) involves assuming a depth and source time function and computing the theoretical weights of each fundamental term for incremental values of strike, dip, and rake. Acceptable orientations are defined by being within some error. This method is useful for preliminary analysis of several hypothesis of depth and time function on good waveform data of any type.

The grid method restricts solutions to be dislocations since dislocation parameters are explicitly used to find the weighting coefficients. This nonlinear parameterization may be linearized by simply allowing any set of weighting coefficients. This is identically equivalent to assuming a purely deviatoric moment tensor point source. Parameterizing the far-field time function as a series of weighted boxcar functions and using the moment tensor formalism allows for a useful linearized least-squares inversion in which smoothness constraints on the time function may be explicitly introduced. These constraints tend to counter unknowns in the earth structure by minimizing trade-offs between time function shape and Green's function shape. However, the moment tensor source model contains more degrees of freedom than the dislocation model so that there may be problems in interpreting results. Double couple constraints on the moment tensor are explicitly introduced by simply incorporating the appropriate derivatives of the moment tensor elements for a shear dislocation with respect to strike, dip, and rake. By independently performing the grid testing inversion and linearized moment tensor or dislocation inversion, one may gain a more useful appreciation for the nature of data and parameter constraints not necessarily obtainable by considering each inversion technique alone.

The development of these interpretation techniques is, in part, motivated by some unusual long-period data recorded at the WWSSN station POO (Poona, India) from several small ($M \sim 4.5$) earthquakes associated with the Koyna Reservoir. Figure 1 displays three components of long-period ground motion at POO for three events on 13 September 1967. These events were the first serious earthquakes associated with the impoundment of the Koyna Reservoir and preceded the major $M6.4$ earthquake

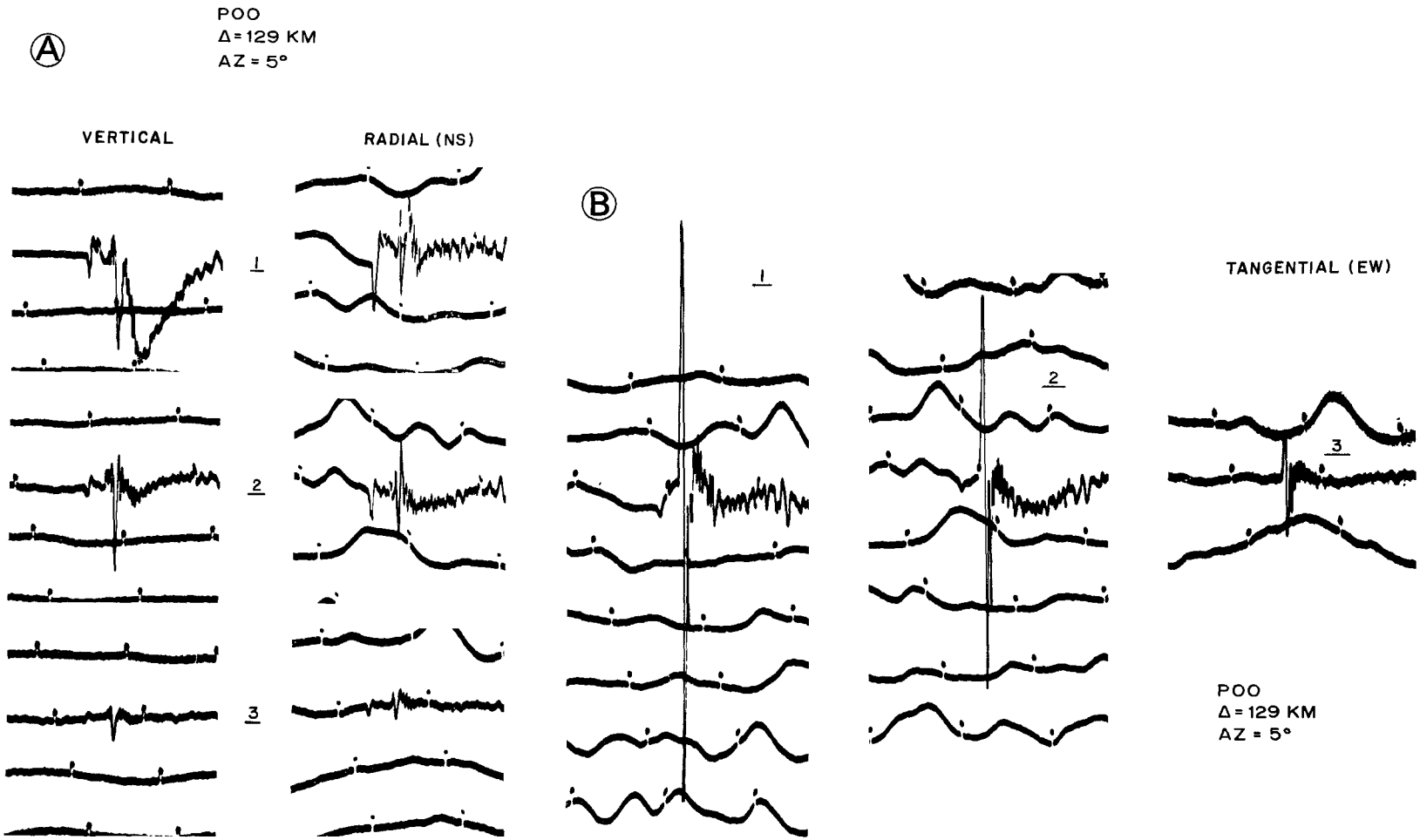

FIG. 1. (a) Vertical and north-south long-period waveforms recorded at POO (Poona, India) for events 1 to 3 of 13 September 1967. The *tick marks* are spaced 1 min apart. The long-period pulse seen on the vertical for event 1 is due to instrument nonlinearity (b) East-west long-period waveforms for events 1 to 3.

which occurred there on 10 December 1967. Although these events are not significant in terms of strain energy release, compared to the main Koyna earthquake, they nevertheless offer clues to the nature of faulting and stresses in the Koyna region which may shed some light on the occurrence of induced seismicity. Unfortunately, the fact that these particular events were poorly recorded at other WWSSN stations precludes first-motion studies or other focal mechanism techniques which rely on large data sets. We are therefore forced to develop techniques which utilize as much source information as possible from waveform data at one or a few stations. Ideally, we wish to estimate and place bounds on source parameters such as depth, fault orientation, and time function. The degree to which this may be done will depend on the data, seismic noise, unknowns in the earth structure, and the parameters themselves.

Theory

The principal results of the dislocation source theory presented in Helmberger (1974) and Langston and Helmberger (1975) can be given by the following equations for cylindrical displacements

$$w(t, r, z, \theta) = s(t) * \sum_{i=1}^{3} \tilde{H}_{w_i}(t, r, z) A_i(\theta, \lambda, \delta)$$

$$q(t, r, z, \theta) = s(t) * \sum_{i=1}^{3} \tilde{H}_{q_i}(t, r, z) A_i(\theta, \lambda, \delta)$$

$$v(t, r, z, \theta) = s(t) * \sum_{i=1}^{2} \tilde{H}_{v_i}(t, r, z) A_{i+3}(\theta, \lambda, \delta) \tag{1}$$

where $s(t)$ is the normalized far-field source time function and (*) denotes convolution. The $\tilde{H}_{d_i}$ where $d = w$, q, or v, can be considered to be Green's functions for an applied step-function dislocation at a point for vertical strike-slip, vertical dip-slip, and 45°-dipping dip-slip (at 45° azimuth) dislocation orientations. This interpretation applies to the $i = 1$, 2, and 3 terms, respectively. The decomposition, which is valid for all exact or approximate wave fields, falls naturally from the displacements given in terms of the Laplace transformed scalar P, SV, and SH potentials. Definitions for the A_i can be found in Langston and Helmberger (1975).

For calculation of near-regional waveforms used in this study, the far-field asymptotic approximations for the potentials [equation (6), Langston and Helmberger, 1975] will be used in conjunction with generalized ray techniques outlined by Helmberger (1968, 1974). Thus, with this particular asymptotic approximation, the $\tilde{H}_{w_i}$ and $\tilde{H}_{q_i}$ will conveniently contain only P-SV potentials and $\tilde{H}_{v_i}$ only SH.

The Green's functions in (1) will be, in general, nonlinear functions of layered elastic parameters and source depth. The orientation parameters, strike, dip, and rake are also included in nonlinear functions. However, the A_i's are simple trigonometric functions to evaluate so that in cases where the $\tilde{H}_{d_i}$ can be calculated from good estimates of structure parameters and source depth and where $s(t)$ is known, the coefficients A_i may be systematically computed for incremental values of θ, λ, and δ. The resulting synthetic displacements may be compared to observed displacements using least-squares or other types of objective functions. For modeling long-period teleseismic body waves or long-period near-regional waves, source depth and $s(t)$ are unknowns which can be of direct interest. Several assumptions of depth and time function must therefore be used with a repeated application of the grid testing.

This is similar to a previously suggested technique (Langston, 1979) made for analysis of long-period body waves. Simplifying assumptions on the ray decomposition in that work can be avoided entirely by computing the appropriate body wave, $\tilde{H}_{d_i}$, responses.

Gilbert's (1970) moment tensor representation for kinematic stress-drop sources has received wide attention in recent years primarily because it elegantly describes the response for a point seismic source in terms of linear combinations of Green's functions, (e.g., see Geller, 1976; Stump and Johnson, 1977; Strelitz, 1978; Mendiguren, 1977). It is straightforward to show that since a purely deviatoric moment tensor is the sum of at least five double couples (see, e.g., Geller, 1976), a purely deviatoric point source can be represented by

$$w(t, r, z) = s(t) * \sum_{i=1}^{3} \tilde{H}_{w_i}(t, r, z)A_i'$$

$$q(t, r, z) = s(t) * \sum_{i=1}^{3} \tilde{H}_{q_i}(t, r, z)A_i'$$

$$v(t, r, z) = s(t) * \sum_{i=1}^{2} \tilde{H}_{v_i}(t, r, z)A'_{(i+3)} \tag{2}$$

where

$$\begin{aligned}
A_1' &= \tfrac{1}{2}(M_{22} - M_{11})\cos 2(AZ) - M_{12}\sin 2(AZ) \\
A_2' &= M_{13}\cos AZ + M_{23}\sin AZ \\
A_3' &= \tfrac{1}{2}(M_{11} + M_{22}) \\
A_4' &= \tfrac{1}{2}(M_{11} - M_{22})\sin 2(AZ) - M_{12}\cos 2(AZ) \\
A_5' &= M_{23}\cos AZ - M_{13}\sin AZ.
\end{aligned} \tag{3}$$

The Green's functions in (2) are the same as in (1) since equations (2) are combinations of equations (1) with different coefficients.

For completeness and because this result will be used in the inversion method, the moment tensor for an arbitrarily oriented dislocation is given by

$$\begin{aligned}
M_{11} &= \sin^2 S \sin\lambda \sin 2\delta + \sin 2S \cos\lambda \sin\delta \\
M_{22} &= \cos^2 S \sin\lambda \sin 2\delta - \sin 2S \cos\lambda \sin\delta \\
M_{12} &= -\tfrac{1}{2} \sin 2S \sin\lambda \sin 2\delta - \cos 2S \cos\lambda \sin\delta \\
M_{13} &= \cos S \cos\lambda \cos\delta + \sin S \sin\lambda \cos 2\delta \\
M_{23} &= -\cos S \sin\lambda \cos 2\delta + \sin S \cos\lambda \cos\delta \\
M_{33} &= -M_{11} - M_{22}.
\end{aligned} \tag{4}$$

Equations (4) are consistent with the results of Mendiguren (1977) allowing for differences in coordinate conventions. Strike, S, is the angle between the x_1 axis and strike of the fault plane in a counterclockwise sense.

Inversion of earthquake seismic data for source parameters is a difficult process and should proceed in a conservative manner. Ideally, it would be desirable to have a general source parameterization, such as an unrestricted moment tensor source, in

which the data would naturally constrain the appropriate physical parameters which could then be clearly interpreted. However, this is rarely the case in seismology. Interpretation of seismic data usually proceeds as a series of hypothesis tests in which "reasonable" assumptions are made to the nature of the source and to the nature of the wave propagation. Often, these "reasonable" assumptions are very good, e.g., the existence of a free surface on the earth, but just as often they may be less applicable to the problem.

In the case of moment tensor source inversion, the allure of the method is mainly in its superficial linear character in which standard linear inverse techniques can be easily applied. This must be weighed against the number of needed assumptions to make the method work and the number of "reasonable" free parameters inherent in the model. For example, many authors have commented that direct physical interpretation of non-double couple terms in earthquake moment tensor solutions is a major problem, although a valid mathematical result (e.g., Stump and Johnson, 1977; Strelitz, 1978). It is not clear, e.g., when, often recognizable unknowns in earth structure are contaminating the source model through nonlinear parameter trade-offs. In a nutshell, these problems arise not because the technique is intrinsically bad, but because the inversion process was not engineered to be consistent with *a priori* assumptions, biases, and acceptable models that are current in the seismological community or in the researcher's mind.

The philosophy that will be followed here is that the source inversion method must give the "smoothest" answer possible in the face of probable unknowns in earth structure. This means minimizing the number of variables and placing constraints on sets of variables consistent with perceived limitations on the data. Stump and Johnson (1977) suggest a time domain method of linear inversion of waveforms using the moment tensor if the source time function of each M_{ij} element is known. In case $s(t)$ is unknown as well, they suggest a point-by-point linear inversion for M_{ij} in the frequency domain. This amounts to a self-consistent deconvolution procedure where the Green's functions are deconvolved from the data. They showed that both of these methods worked well for synthetic data in which the earth structure effects were completely known. However, both of these methods sacrifice several desirable aspects to the end of keeping the problem linear. The frequency domain method can allow considerable trade-off of time function with the effects of unknown earth structure in the Green's functions through the inclusion of six free parameters for every frequency point. It would be useful to have a way of constraining the duration of possible time functions, of smoothing time domain shapes, and of limiting the number of parameters. The time domain method may be more pleasing in this respect since there is absolute control over time function, but if the time function is the object of the inversion this becomes of limited use. Lastly, for earthquake modeling, there should be some direct connection to standard double couple parameters to at least provide continuity with past source studies and to provide a framework to interpret the moment tensor results. This means directly placing constraints on the inversion to obtain double couple parameters rather than interpreting a moment tensor for pressure and tension axes. Strelitz (1978) clearly demonstrated the problems with this latter procedure.

The form of the inversion for both moment tensor and dislocation parameters will be based around equation (2). The far-field time function, $s(t)$, will be assumed to be common to each moment tensor element although this is not a restriction on the method. The time function will be parameterized as a series of boxcar elements with differing weights. The width of each boxcar is specified to be $\Delta\tau$ so

$$s(t) = \sum_{i=1}^{n} s_i B(t - \tau_i) \tag{5}$$

where

$$B(t - \tau_i) = H(t - \tau_i) - H(t - \tau_{i+1})$$

and

$$\tau_i = \Delta\tau(i - 1).$$

The width, $\Delta\tau$, is specified by considering the bandwidth of the data. For example, $\Delta\tau$ was set to 0.5 sec for inversions using long-period WWSSN waveform data; the difference between an impulse and a half-second boxcar function is almost negligible when these functions are convolved with the long-period instrument response.

Equations (2) may be rearranged using (3) to produce new Green's functions multiplied explicitly by each moment tensor element. Also including (5), the vertical displacement becomes, e.g.,

$$w(t, r, z) = \sum_{i=1}^{n} s_i B(t - \tau_i) * \sum_{j=1}^{5} \tilde{H}'_{w_j}(t, r, z) M_j' \tag{6}$$

where,

$$M_1' = M_{11}$$
$$M_2' = M_{22}$$
$$M_3' = M_{12}$$
$$M_4' = M_{13}$$
$$M_5' = M_{23}$$

and, e.g.,

$$\tilde{H}'_{w_1} = -\tfrac{1}{2}\tilde{H}_{w_1}\cos 2(AZ) + \tfrac{1}{2}\tilde{H}_{w_3}.$$

Regrouping the time dependent terms

$$w(t, r, z) = \sum_{i=1}^{n}\sum_{j=1}^{5} s_i M_j'[B(t - \tau_i) * \tilde{H}'_{w_j}(t, r, z)]. \tag{7}$$

Similar equations are obtained for the other displacements. The object of the inversion is to determine the coefficients, s_i and M_j'. A standard iterative least-squares procedure (Wiggins, 1972) is used to invert these equations given corresponding waveform data. From (7), it is clear that the first partial derivatives of a synthetic waveform with respect to the s_i or M_j' will be dependent on the chosen starting model. However, there are only cross-second derivatives with no pure second derivatives. Numerous trial inversions on synthetic three-component waveform data similar to the data of Figure 1 showed that convergence was fast, occurring within about five iterations, and displayed no adverse dependence on starting model.

The advantages of parameterizing the time function as in (5) lie principally in the control afforded over time function duration and shape. *A priori* information on the duration is simply included by specifying the number of boxcar elements. Smoothing

may also be added by explicitly averaging elements by a linear or spline method; this is done in the data inversions. Both smoothing and duration control reduce the number of inversion parameters leaving the essential shape information unchanged and allowing greater control over the inversion. Trade-offs can still occur between unmodeled earth structure and time function behavior, however, and must be investigated by changing assumptions on earth structure. An additional least-squares constraint is introduced to keep the time function area unity in the manner suggested by Jackson (1979).

Explicit inversion for the dislocation parameters, strike, dip, and rake, is easily accomplished by taking the necessary derivatives of the moment tensor elements [equations (4)]. These are included in the synthetic seismogram equations [e.g., equation (7)] where needed. Thus, with very little extra work, dislocation parameters

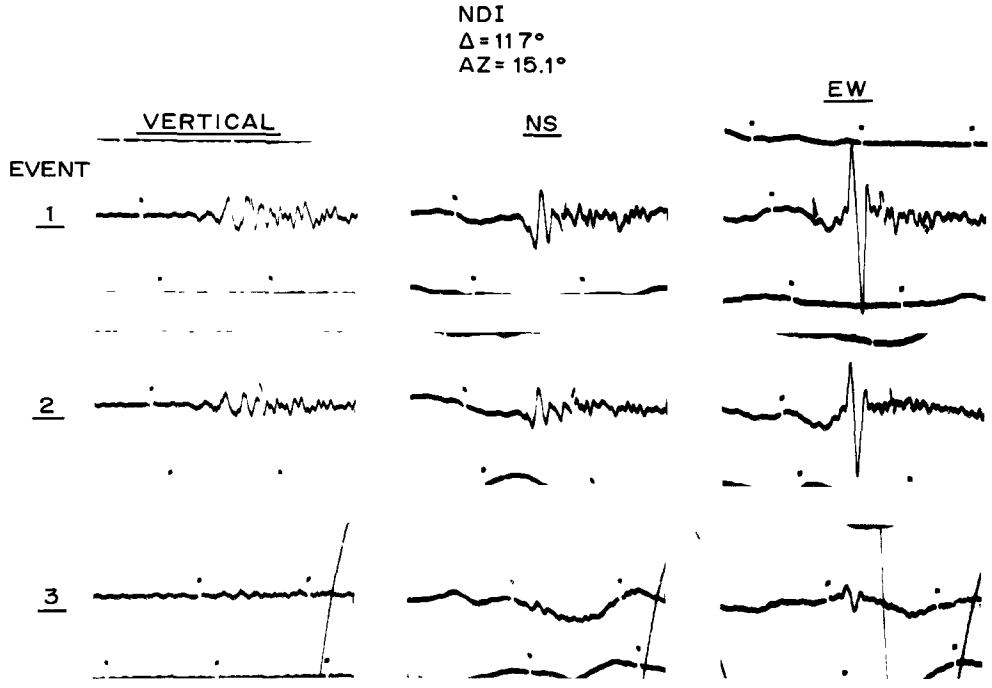

FIG. 2. Vertical, NS, and EW long-period ground motion at NDI (New Delhi, India) for events 1 to 3 on 13 September 1967 Note the striking similarity of waveshapes between events. Peaks later in the coda may even be correlated indicating that mechanism and locations are nearly identical for all three events.

may be solved for in the same manner as unrestricted moment tensor elements. Both inversions could be done as a matter of routine and would aid in data and source model interpretation. Trials using synthetic data in which time function and dislocation parameters were both inverted indicated that convergence was just as rapid as in cases when unrestricted moment tensor elements were used. However, because the dislocation derivatives are sinusoidal in character, there was a marked dependence of starting model on stability; starting models within about $\pm 20°$ of the true orientation angles converged to the true answer quickly but radically different orientations caused divergent or oscillating behavior in the solution as iterations were performed. These tests were not comprehensive and were performed on synthetic data similar to the waveforms of Figure 1. Note that this is an alternative and direct way to explicitly constrain the moment tensor to yield double couple

parameters compared to methods involving equations of constraint suggested by Mendiguren (1977) and Strelitz (1978).

Data and Data Analysis

The moderate earthquakes of 13 September 1967 were the first serious events associated with the impoundment of the Koyna Reservoir (Narain and Gupta, 1968; Guha *et al.*, 1970). Figures 1 and 2 show the three components of ground motion recorded at the WWSSN stations POO and NDI for three discernable earthquakes of that day. Figure 3 is an index map of the area. Table 1 presents the source

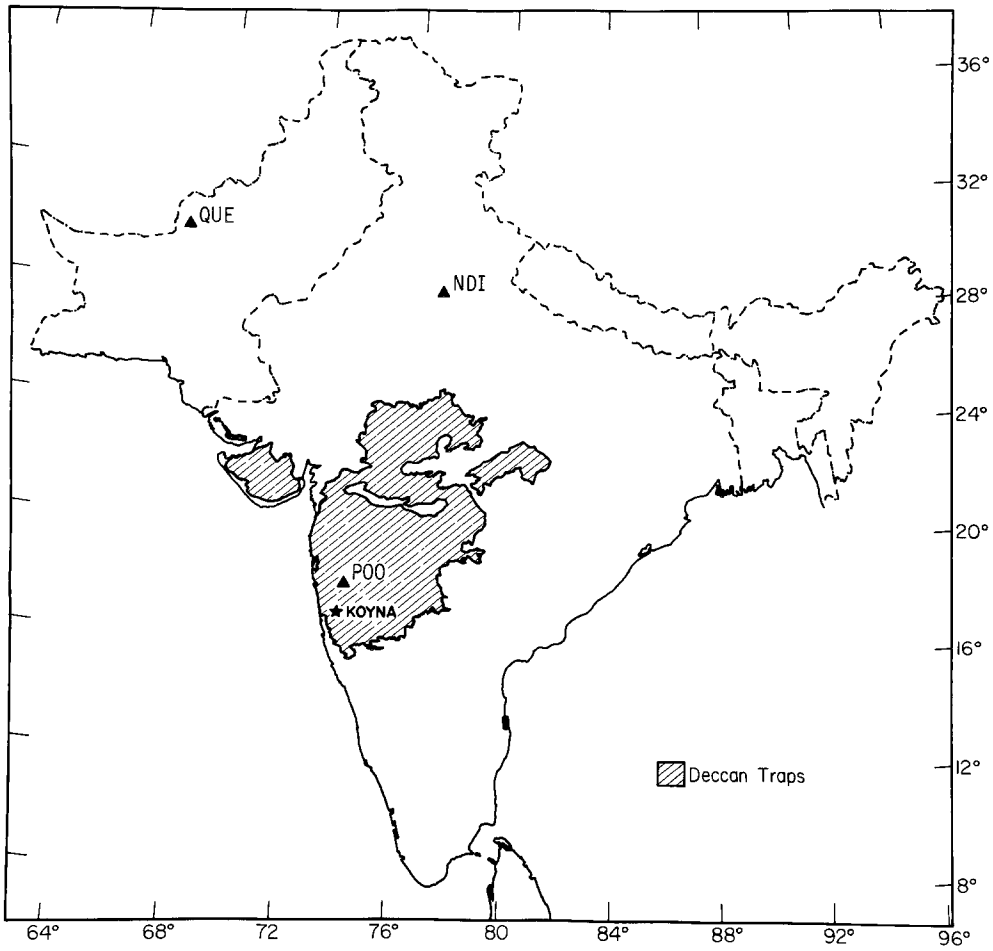

FIG. 3. Index map showing source and station locations.

parameters determined by ISC and Guha *et al.* (1970). These three events show several unusual characteristics. The first obvious one is the striking similarity of waveform shapes and relative amplitudes beween events as seen on the POO and NDI recordings. Aside from long-period noise and nonlinear instrument effects (e.g., POO vertical component for event 1), waveforms between events may be superimposed and show a peak-for-peak correlation even into their codas. This strongly suggests that source orientation and location are common to each event. Location must be within about a 2-km radius to sustain the same observed interference of low group velocity (~2 km/sec) scattered coda waves of a roughly 2- to 3-sec period.

Source orientation must also be similar to sustain this interference and the more obvious similarities in the major arrivals. This then suggests that the three events are associated with the same fault and are a result of repeated movements at nearly the same point on the fault. Short-period recordings at NDI (not shown) are also strikingly similar between events 1 and 2 and show the same relative amplitude ratio between events as the long-period recordings.

Guha *et al.* (1970) assigned a magnitude of 5.8 to the first event based primarily on interpretation of maximum acceleration data and intensity. The other two events were assigned magnitudes of 4.5 (Table 1). There is an obvious disparity between these assigned magnitudes and the observed event relative amplitudes. Table 2 displays several magnitude calculations based on different waves and magnitude scales for events 1 and 2. On the basis of the few stations which recorded these events, it is difficult to assign a particular magnitude with any confidence. Nuttli's (1973) M_S for 3- to 12-sec Rayleigh waves and m_b for 1-sec vertical *Lg* waves for eastern North America are included for comparison with the IASPEI M_S results.

TABLE 1

STANDARD SOURCE PARAMETERS FOR THE KOYNA EARTHQUAKES OF 13 SEPTEMBER 1967

Event	Date	Origin Time	Latitude (°)	Longitude (°)	Depth (km)	LSC	Magnitude*
1	13 September 1967	$06^h\ 23^m\ 31^s$	17.6	74.0	4	5½–6†	5.8
2	13 September 1967	$06^h\ 48^m\ 25^s$	17.4†	73.7†	4†	5½–6†	4.5
3	13 September 1967	$07^h\ 00^m\ 28.2^s$	—	—	—	—	4.5

* Source: Guha *et al.*, 1970.
† Parameters given by NDI

TABLE 2

MAGNITUDE DETERMINATIONS

Event	M_S (IASPEI)		M_S*	m_b*
	NDI	QUE	NDI	NDI
1	4.8	3.6	4.1	5.2
2	4.6	3.4	3.9	5.1

* Source: Nuttli, 1973.

These numbers suggest, however, that events 1 and 2 are closer to magnitude 4 to 4.5 rather than the previously believed 5.5 to 6. Based on the event amplitude ratios observed in Figures 1 and 2, events 2 and 3 have relative magnitude differences of −0.2 and −0.8, respectively, compared to event 1.

At the time of these earthquakes, there were seven short-period seismic stations operating in a relatively tight net around the Koyna Reservoir (Gupta and Coombs, 1976). However, most located events lie outside and to the south of the network several kilometers from the dam site. Experience with small seismic networks indicate that source locations and especially depths may have large errors when outside the network perimeter (Peters and Crosson, 1972). Thus it would be desirable to have an independent depth determination for these earthquakes along with estimates of orientation parameters.

Intuitively, to model source parameters, one would like to choose seismic data in which the structure effect on waveforms is at a minimum or at least predictable and where source time function and radiation pattern is easily discernable. Using this reasoning, the long-period surface wave data of NDI and QUE were discarded since

detailed dispersion and structure characteristics for paths from Koyna to these stations are not known with the precision needed to match amplitudes and phase. The data from Poona, on the other hand, is simple in character reminiscent of solutions to Lamb's problem. The vertical and radial (NS) components of Figure 1 show apparently simple *P* and Rayleigh wave arrivals. The tangential (EW) appears to be composed of a simple *SH* pulse. We will, therefore, use the waveform data at POO to estimate orientation, time function, and source depth through inversion of synthetic seismograms using the techniques outlined in the previous section.

Crustal structure in the Koyna area is known primarily from Rayleigh wave dispersion measurements, earthquake travel-time studies, regional gravity interpretation, and shallow refraction measurements (Narain, 1973; Kailasam *et al.*, 1969). Table 3 presents two crustal models used to construct Green's functions for inversion. Model B is a two-layer crust model constructed from velocity measurements and thicknesses given by Narain (1973) and is similar to a model used by Langston (1976). The shear wave velocity is reduced slightly in model B compared to velocities given by Narain (1973). This was needed to reproduce the correct *S-P* and Rayleigh-*P* times as seen in the data. Model D is a one-layer approximation to the two-layer model constructed by preserving vertical travel times in the crust and having the same Moho velocity contrasts. Model B should represent a fair approximation to

TABLE 3

KOYNA CRUST MODELS

Model	Layer	*Vp* (km/sec)	*Vs* (km/sec)	ρ (gm/cm^3)	Th (km)
D	1	6.0	3.5	2 7	38.5
	2	7.6	3.9	2.9	Half-space
B	1	5.7	3.3	2.7	20.0
	2	6 5	3.8	2.9	20.0
	3	8.2	4 7	3.2	Half-space

the structure at Koyna. A layer representing the Deccan trap basalts was not included because observed *P*-wave velocities in the basalts quickly attain comparable high velocities at depths of a few hundred meters (Kailasam *et al.*, 1969). Velocities near the surface range from 4.8 to 5.2 km/sec so the near-surface layer should have little effect on wave propagation in the band of the long-period WWSSN system. Model D is included primarily to investigate the effect of assuming an inferior Green's function in the inversion process. The path from Koyna to POO (Figure 3) lies within the Deccan Plateau and nearly parallels the coast. Thus, there are no obvious topographic or lateral structural discontinuities to complicate the wave propagation.

Event 2 waveforms from POO were used exclusively in the following inversions. Event 1 data show obvious nonlinear instrument effects on the vertical component, a large amount of long-period noise on the radial, and a large, faint (on original recording) *SH* pulse which was difficult to digitize. Vertical and radial waveform data for event 3 are low amplitude and obscured by trace-line thickness. Compromising between these problems, event 2 waveforms were digitized at an equal time increment of 0.25 sec. The data were detrended by least-squares fitting a third-degree polynomial to each trace and subtracting the result. This amounted to a simple baseline shift for the vertical component, but was significant in removing

much of the visual long-period drift on the radial. Because the arrivals of interest are of much shorter duration than the long-period drift, these corrections produced little pulse distortion. Rotation of the horizontal components into the theoretical back azimuth had a negligible effect on the amplitude or shape of the EW component, but proved to be unstable for the radial Rayleigh wave. Because of the large *SH* amplitude, small uncertainties in relative time shifts between EW and NS components caused significant radial Rayleigh wave shape differences. Thus the

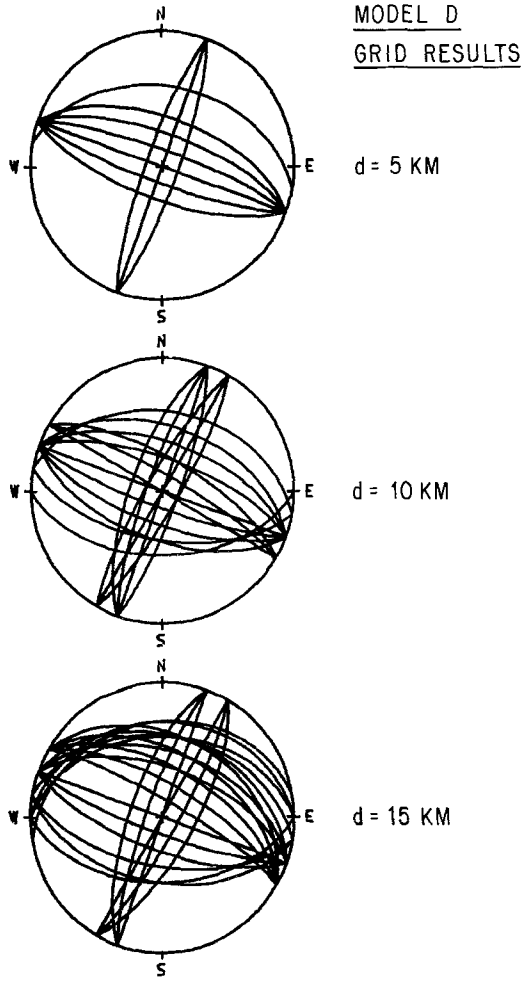

FIG. 4. Lower hemisphere equal area projections showing acceptable fault plane solutions for depths of 5, 10, and 15 km using the grid method and model D. All mechanisms are left-lateral on the NNE striking planes. Orientation angles were incremented by 10°

radial Rayleigh arrival was not used. We expect nearly the same source information to be contained in the larger and clearer vertical Rayleigh wave. The final detrended waveforms are displayed in Figures 6 and 7.

In addition, a suite of teleseismic waveforms recorded at POO was collected to check the polarities and calibration characteristics of the long-period system. Based on known source locations, long-period *P*-wave polarities and amplitudes indicated no obvious instrument polarity reversals or miscalibration. Calibration pulse ampli-

tude and shapes were also normal. Comparison of the vertical and horizontal components for P waves from simple deep events also indicate no anomalous crustal structure under POO; P to S conversions were relatively small and there was little evidence of off-azimuth converted arrivals (Burdick and Langston, 1977; Langston, 1977). Thus, there is no evidence to expect instrument problems or trouble with the plane-layered approximation for computing Green's functions.

The polarity and relative amplitude of radial P, tangential SH, and the positive and negative maxima of vertical Rayleigh were read from the data and normalized

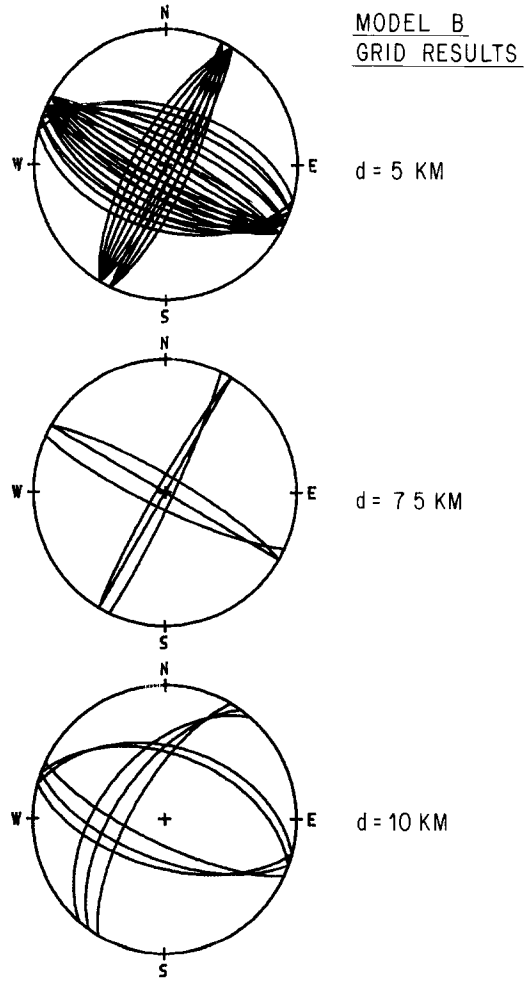

FIG 5 Grid method results using model B. Same scheme as Figure 4 except that the angle increment is now 5°

relative to the SH wave. These amplitude ratios and polarities were then tested against theoretical ratios and polarities computed systematically from Green's functions convolved with a trial 1.5-sec duration boxcar time function and the WWSSN instrument response. The objective function used required that all polarities must agree and that amplitude ratios lie within a value σ_i defined by

$$\sigma_i \geqq \left| \frac{o_i - c_i}{o_i} \right| \tag{8}$$

where o_i and c_i are the observed and calculated amplitude ratios for the ith measurement, respectively. Figures 4 and 5 show the acceptable solutions obtained for a σ_i of 0.4 for the P/SH and P/Rayleigh (negative) maximum ratios, and 1.0 for the P/Rayleigh (positive) maximum ratio for models D and B, respectively. All solutions indicate left-lateral strike-slip motion along the NNE trending set of nodal planes. Assuming model D, Green's functions leads to a greater number of acceptable orientations as depth increases. This effect is reversed, however, when model B Green's functions are used. It is also somewhat surprising that this technique is as robust as it seems to be since similar solutions are obtained with different Green's functions. Previous testing of the method with synthetic data based on models B and D did show that orientation angles could generally be well constrained to at worst ±15° with similar assumptions on the σ_i. The only significant trade-offs

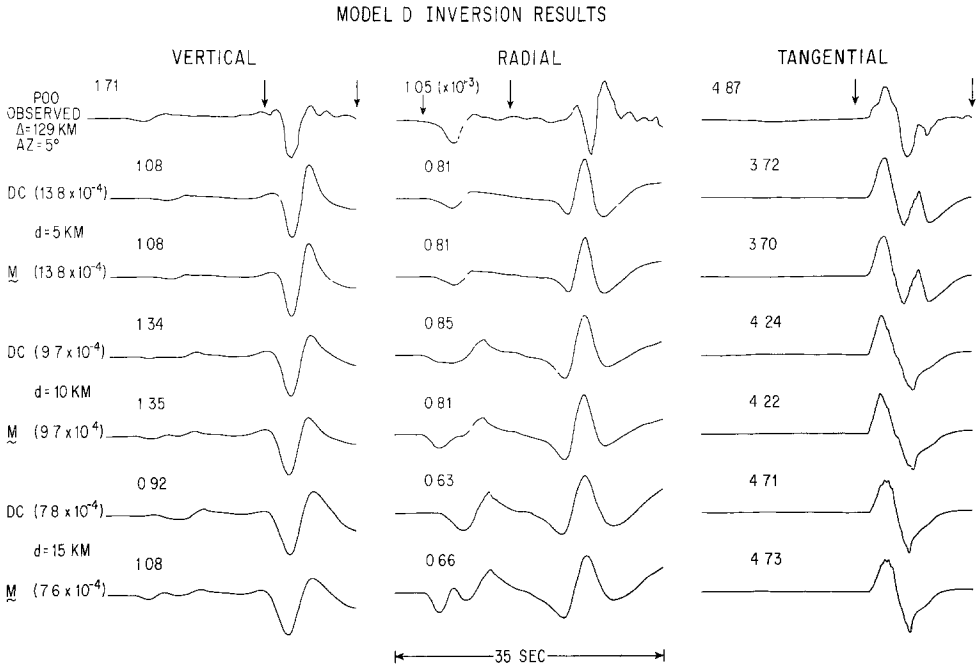

FIG. 6. Observed (*top*) and synthetic (*below*) vertical, radial, and tangential waveforms from moment tensor and dislocation inversions for several depths using earth model D. Amplitudes are in centimeters. The number to the *left* of each triad of synthetic waveforms is the rms error of the residual from each inversion. The arrows delimit the data windows used in the inversions.

observed in these single-station tests were between vertical strike-slip and 45°-dip-slip solutions for some station azimuths away from nodal plane directions. In fact, the best constraint is on strike for the NNE planes of Figures 4 and 5 and is mainly a function of the large observed *SH* waves relative to *P* and Rayleigh.

The grid testing suggests that faulting was left-lateral strike-slip on the NNE-trending planes or right-lateral on the NNW planes with the possibility of substantial oblique motion. However, to estimate time function and depth parameters, waveform shape and arrival information must be utilized in conjunction with the gross amplitude behavior. Figures 6 and 7 display the results of moment tensor and double couple waveform inversions with assumption of models D or B, respectively. Figures 8 and 9 show the final double couple and interpretation of the moment tensor for

the greatest double couple for each inversion. Table 4 lists relevant inversion parameters for each trial.

A maximum duration of 3.5 sec was chosen for the far-field time function based on previous trial-and-error waveform modeling of the data and also on theoretical considerations of what expected pulse widths (or corner frequencies) for events of this size should be (Helmberger and Johnson, 1977; Kanamori and Anderson, 1975). Thus, seven boxcar elements were used. A simple linear smoothing scheme was incorporated whereby the amplitude of each even numbered element was explicitly given as the average of adjacent elements. Thus, the moment tensor source inversions had a total of nine free parameters, and the dislocation source inversions only seven free parameters. The number of waveform data points was approximately 150.

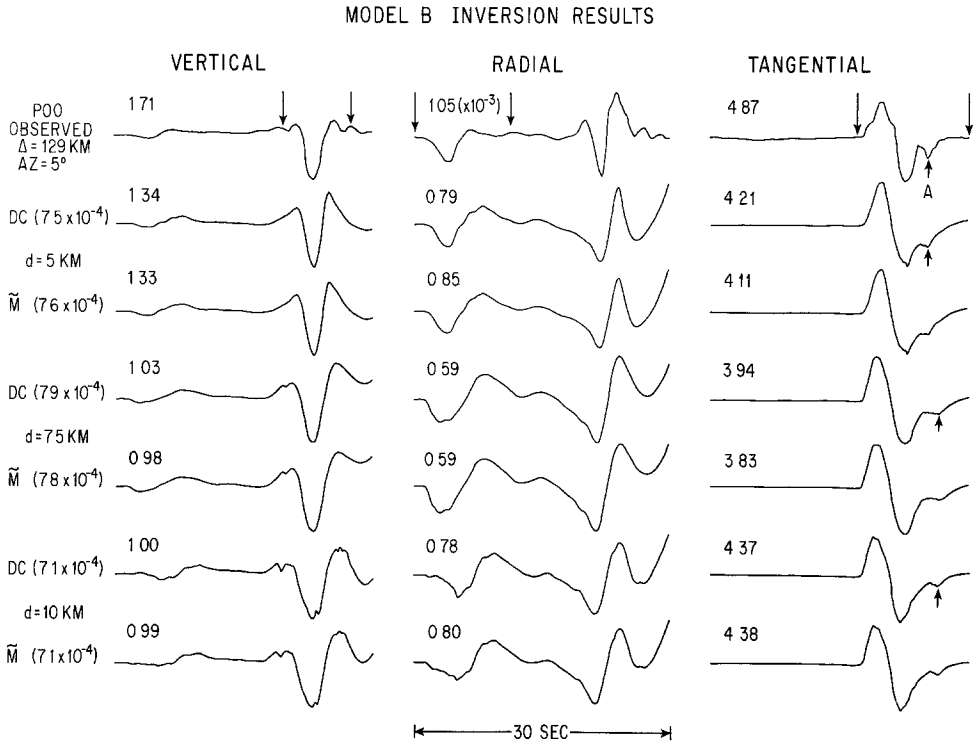

FIG. 7. Model B inversion results, same scheme as Figure 10 The phase marked "A" is an inferred depth indicator discussed in the text.

In applying the inversion technique, it was found that data and Green's function time windowing was a useful way to control and choose which data were to be used and to reduce the dependence of knowing absolute arrival times. The portions of the observed waveforms between arrows in Figures 6 and 7 were those used as data in the inversions. The windowed data were shifted in time, relative to corresponding arrivals in the Green's functions, so that models with obvious deficiencies in relative timing could be used, such as with model D between P and Rayleigh. The wisdom of using this technique is obvious for many seismic arrivals, i.e., far-field teleseismic P or S waves, but may be questionable when dealing with the interference effects of regional reflections and refractions. Therefore, inversions with model D must be considered an experiment in which the time shifting is done in the same spirit as choosing amplitudes from the various waves in the grid technique.

Several characteristics are common to both sets of inversions. First, because the *SH* wave is so large relative to other components, the least-squares technique tended to favor it. As a result of this, the rms of the residuals or rms error tended to be very similar for all inversions; there did not seem to be any obvious numerical criteria for determining which model was best. A weighted least-squares was tried to counteract this, but very similar results were obtained. Second, in almost all cases, the dislocation model gave identical waveform fits as the moment tensor model. The

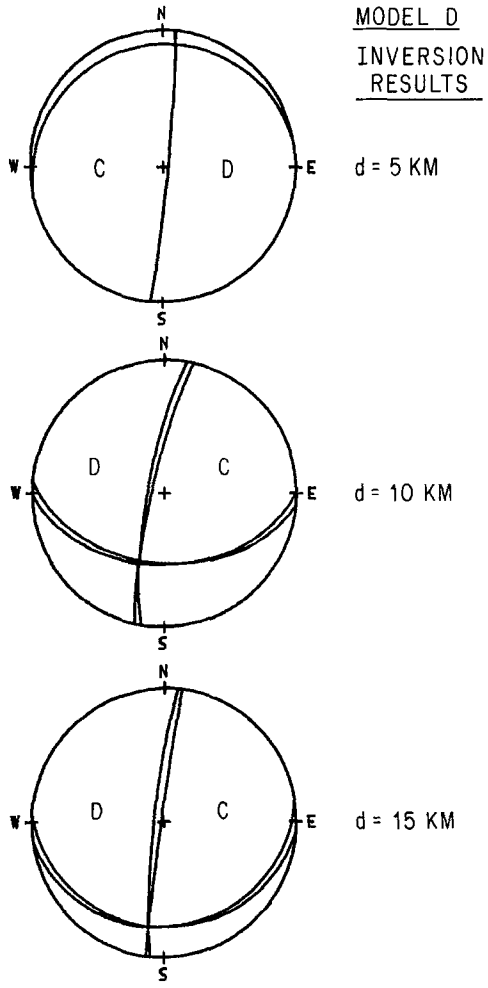

FIG. 8. Interpreted moment tensor and double couple orientations determined from model D inversions.

greatest differences are seen only in the radial *P* wave for deeper source depths. Finally, the orientation found from the dislocation inversion always agreed well with the greatest dislocation contained within the moment tensor solution. The moment tensor was interpreted by rotating it into its principal axes, decomposing the result into the greatest double couple and a remainder compensated linear vector dipole (CLVD) source, and using the pressure and tension axes of the double couple to infer strike, dip, and rake. Table 4 lists double couple and interpreted moment

tensor orientations for each inversion and the percentage CLVD source contained within the moment tensor. The percentage is based on the ratio of the seismic moments of the decomposed double couple and CLVD. Inversions based on this data set, therefore, do not display the instability of deduced pressure and tension axes discussed by Strelitz (1978) when moment tensor and double couple source inversion models are compared.

Because the inversions are biased toward fitting the large *SH* pulse and all fits are

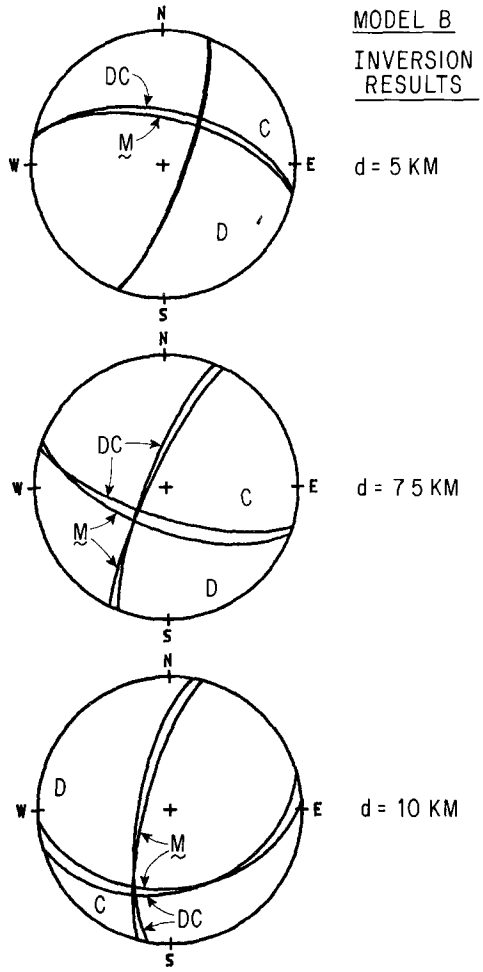

FIG. 9 Model B inversion orientations.

numerically similar, the problem remains of finding a rational method in choosing the best answer in some sense. A purist may say that the final inversion results are the best that may be done and that, indeed, the similarity in fits indicates that the different models are unresolvable. This philosophy overlooks the fact that, at best, any inversion technique is a testing medium of a limited set of hypotheses often defined by the limitations of the technique itself. We, therefore, take a more global view of the problem by imposing *a posterior* constraints based on hypothesis of data noise, Greens' function or earth model quality, results of other types of

inversions, and interpretation of details in the solutions which were largely ignored by the least-squares procedure but may have great intrinsic worth. To this end, we first impose the requirement that waveform inversion models must be consistent with the appropriate grid testing results. This excludes all of model D inversions, most of which yielded nearly vertical dip-slip orientations on a NS plane as compared to vertical strike-slip orientations on a N20°E plane from grid results. Model D may also be excluded on the basis of inferior *S-P* and Rayleigh-*P* times. Inversion results for depths of 10 and 15 km (Figure 10) also show that, although the *SH* pulse duration is approximately correct, synthetic radial *P* waves exhibit anomalous pulse widths and multiple arrivals. Synthetic vertical Rayleigh wave pulse width is also too large for these depths. Waveform inversions based on earth model B for source depths of 5 and 7.5 km are most consistent with the grid results for orientation. Again, as in model D synthetic waveforms, anomalous pulse widening is apparent in the radial *P* wave and vertical Rayleigh wave for source depths greater than 5 km.

TABLE 4

INVERSION MOMENT TENSOR AND DOUBLE COUPLE PARAMETERS

Depth	M_{11} (or M_0) (dyne-cm)	M_{22}	M_{12}	M_{13}	M_{23}	s (°)	δ (°)	λ (°)	CLVD (%)
				Model D					
5 (M)	1 37 ($\times 10^{22}$)	3.95	−9 73	−4.14	47.8	5.4	86.7	79.1	1
5 (DC)	49.4	—	—	—	—	5.5	87.0	79.1	—
10 (M)	4.51	−2.18	−9.15	−0.02	−9 58	192 8	82.2	44.1	8
10 (DC)	13.8	—	—	—	—	190.0	79.6	45.5	—
15 (M)	5.31	−2.94	−9.68	1.28	−24.7	187.8	88 3	66.9	12
15 (DC)	26.9	—	—	—	—	186.0	83.8	67.4	—
				Model B					
5 (M)	5.23 ($\times 10^{22}$)	−2.89	−6.25	4.75	3.85	20.7	76 1	29.5	7
5 (DC)	8.98	—	—	—	—	20.1	77.4	34.6	—
7.5 (M)	7.01	−6.83	−5.98	−0.49	−5.94	206 2	80 0	27.4	21
7.5 (DC)	9.02	—	—	—	—	202.0	77.6	19.2	—
10 (M)	3 82	0.51	−6.15	−0.80	−8.04	194.5	74 6	52.0	13
10 (DC)	11.5	—	—	—	—	190.0	70.5	56.1	—

An added argument for a source depth of 5 km comes from interpreting a secondary arrival in the *SH* wave. An arrival marked "A" in the *SH* waveform of Figure 7 is unintentionally matched well by inversion using the 5-km depth source of model B. In the synthetics, this arrival is caused by critical reflections from the mid-crustal and Moho interfaces of crust model B for *SH* waves which also reflect off the free surface. As source depth increases, travel time to the free surface increases so that the arrival moves back into the *SH* waveform as shown in Figure 7. The 5-km depth moment tensor solution for model B also shows the least non-double couple component of all inversions except for the 5-km depth model D solution. This has been suggested by Mendiguren (1977) as a measure of error in moment tensor inversion of earthquake data.

DISCUSSION

From the foregoing, we conclude that the earthquakes of 13 September 1967 occurred at a source depth of 5 km and, taking one nodal plane, were caused by left-

lateral strike-slip motion on a nearly vertical fault striking N20°E. Analysis of errors for this model is rather difficult since most errors are undoubtedly associated with unknown deficiencies in the Green's functions. Each inversion did display good stability with respect to fast convergence (within five iterations) and low-condition numbers; the ratio of the largest to smallest eigenvalues was generally less than 10. A good approximation for the variability of orientation parameters can be inferred from the grid testing results for the 5-km depth case of Figure 5. For the NNE nodal plane, strike, dip, and rake are constrained to be within about N20°E ± 5°, 90° ±

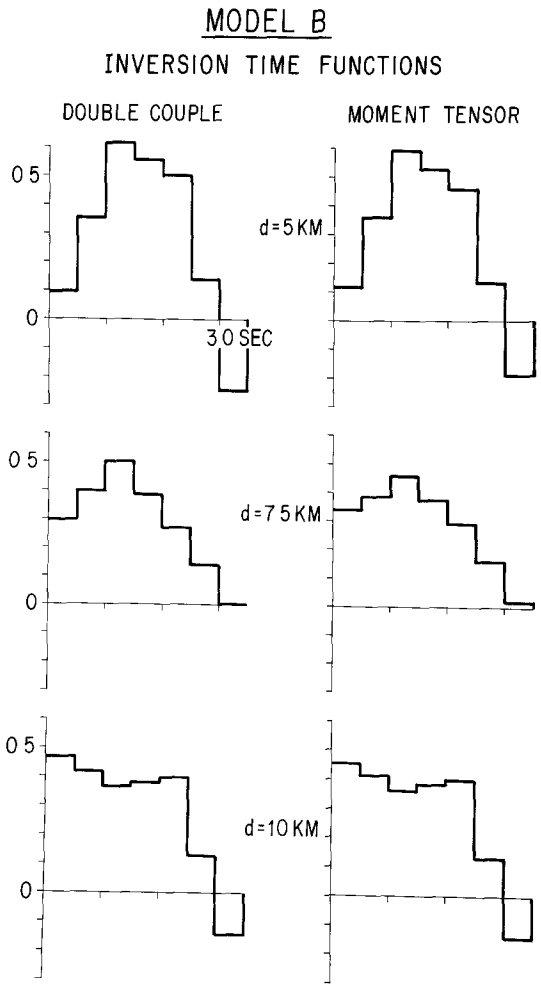

FIG. 10. Time functions determined from model B inversions.

15°, and 0° ± 35°, respectively. This is probably a conservative estimate since the error allowed in the amplitude ratios is large (40 per cent). It is worth noting that this orientation and depth is very similar to that found from an analysis of teleseismic body waves from the main M6.4 December event (Langston, 1976). Source parameters from that study were N16°E ± 6°, 67° ± 6°, and −29° ± 6° for strike, dip, and rake, respectively, for a source at 4.5- ± 1.5-km depth. This strongly suggests that the 13 September and 10 December events all occurred on the same structure.

Variation of time function parameters is harder to evaluate and depends on

unknowns in the Green's functions. From calculation of several synthetic models, the details of the time function for 5-km source depth (Figure 10) are probably unimportant except that it behaves as relatively smooth and simple pulse approximately 3 sec in duration. Also, no particular importance should be attached to the small negative excursion in the time function except that it probably represents a compensation for deficiencies in the Green's functions. This time function is of relatively long duration compared to similar-sized California events. Helmberger and Johnson (1977) found far-field time function durations of about 0.5 sec for events associated with the San Andreas system with seismic moments of 10^{23} dyne-cm. Long-duration low-moment far-field pulses are generally associated with low stress drops using Brune's (1970) model, but this is critically dependent on assumptions of rupture velocities, rise time, and fault area. Assuming Brune's model yields stress drops on the order of 0.05 bar. However, if dislocation rise time predominates over the rupture velocity-fault dimension effect, or if rupture velocity is unusually slow, then stress drops may be much higher and in line with average values (~10 bars) attained by other earthquakes (Kanamori and Anderson, 1975). Nevertheless, these Koyna events display unusually long-duration time functions which, with further study, may possibly be indicative of reservoir-induced earthquakes.

The geology and tectonics of the Koyna region is only partially known. The Koyna Reservoir is located a few kilometers to the east of the Western Ghats, the continental divide for Peninsular India. The Western Ghats is a 1000-m westward-facing escarpment in otherwise flat-lying Deccan Basalts. There has been some discussion as to the origin of this escarpment; whether it is a simple erosional feature or whether it is a result of faulting. From the presence of hot springs and from the step-like topography along the Western Ghats, some researchers favor a model in which the escarpment marks the location of a broad en-echelon zone of deep-seated faults (D. T. Snow, personal communication; Athavale, 1975) and that the Koyna earthquakes were triggered on some of these faults by pore pressure changes when the reservoir perturbed the previously existing hydrogeological regime.

Unfortunately, there is little to document these suspected faults. Available geological maps of India (Roy, 1963) show no faults at all in this area and more recent maps are classified by the Indian government. To work around this difficulty, LANDSAT images for the area were obtained from the USGS and a fault and lineation map was constructed using both black-and-white and color composite images (Figure 11).

The Koyna Reservoir is the sinuous lake near the upper center of the map. Inferred faults are drawn as solid lines and suspected faults are dashed. Inferred faults were interpreted from the images usually on the basis of identifying long linear valleys, straight notches cutting across spurs and ridges, straight stream segments, straight escarpment edges, and combinations of these. Because most of these are erosional features, it is likely many represent fault-line scarps rather than true fault scarps. The faults drawn in Figure 11 probably represent a conservative view of the structure since nearly all represent obvious linear features which were easily identified by several independent interpreters. Suspected faults are more subjective and are based on linearity of tone or color features. More could probably be drawn due to the human eyes' amazing talent for picking order out of chaos. However, only a few of the more obvious lineations that co-workers also saw were used. There is probably a natural bias in the density of the faults as a function of position on the map since most distinct erosional features are associated with the

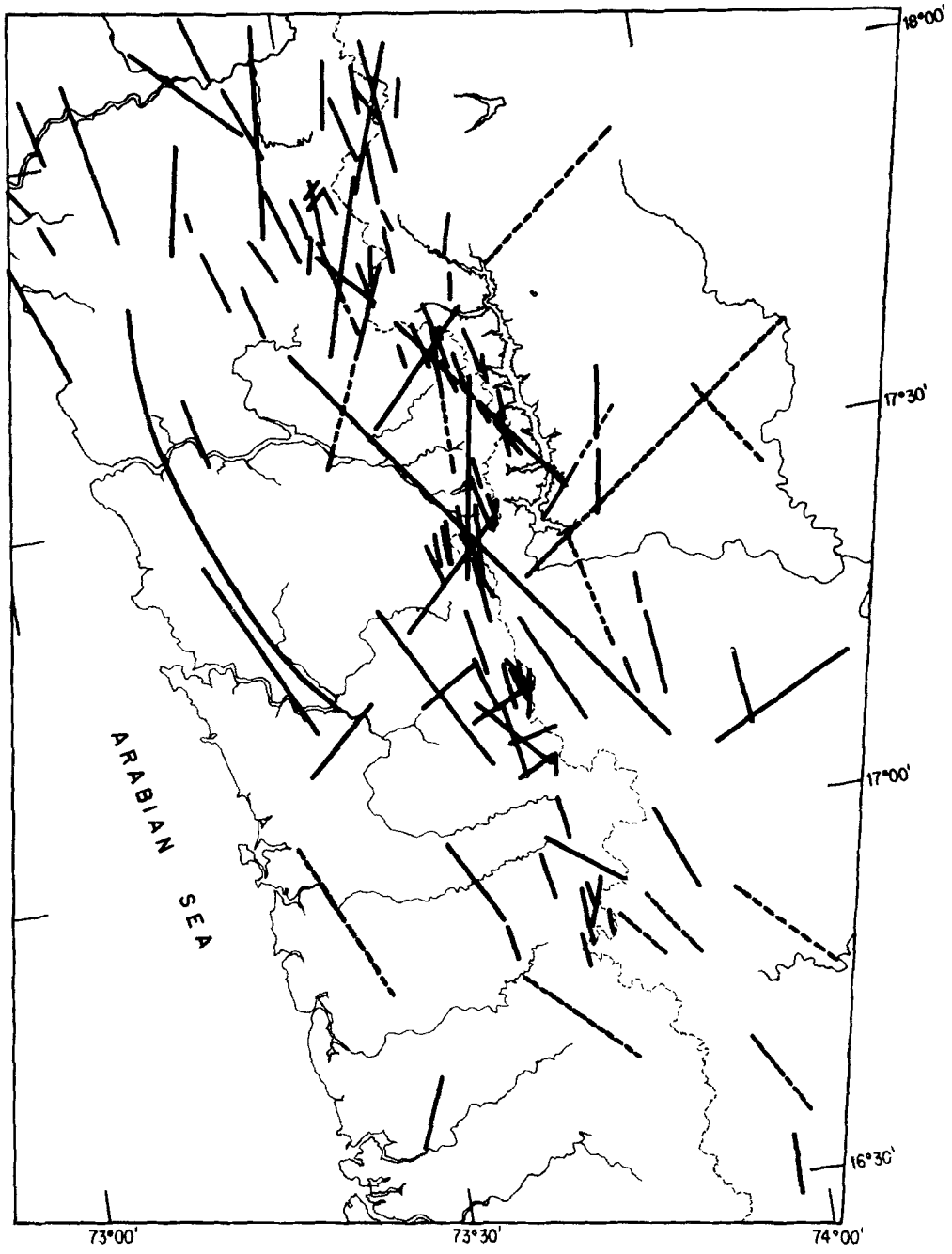

FIG. 11. Fault map for the Koyna region interpreted from LANDSAT images. The solid lines are interpreted to be faults based on unambiguous linear features discussed in the text The dashed lines are tentative identifications of faults. The three 13 September events occurred near the bend of the river just south of the Koyna reservoir.

highest topography along the Western Ghats. Flat areas, especially to the east of the reservoir, were much more homogeneous in color and tone.

The fault map supports the idea that the Western Ghats is the locus of a large zone of en-echelon faults parallel to the coast. Most faults strike in a NNW to NE

azimuth. There are several NNE striking faults and lineations near the dam which are good candidates for the fault or faults which cause the Koyna events of 13 September 1967, and the main event of 10 December. In detail, however, the granitic basement, which is at 1- or 2-km depth (Guha *et al.*, 1976) may have a different fault morphology. Many of the faults seen on the surface may be secondary as a result of small movements of larger scale "wrench" faults in the basement. In any case, this map provides an overview of the large scale structures in the area and suggests that the NNE striking nodal plane found from the inversion is probably the fault plane.

Conclusions

If earth structure is adequately known to enable computation of the appropriate Green's functions, several methods may be used to invert seismic waveforms to obtain moment tensor, dislocation, time function, and other source parameters. One particularly simple method is to perform a nonlinear systematic trial-and-error testing (grid method) of the data assuming source depth and time function. The grid method has the advantage of employing distinctly nonlinear objective functions to find nonlinear parameters. For example, the grid method was used to find dislocation, strike, dip, and rake from observed amplitude ratios and polarities of near regional *P*, Rayleigh, and *SH* waves. This method is useful to quickly test several hypotheses concerning the data. Alternatively, a linearized least-squares inversion may be performed using moment tensor or dislocation sources in the time domain by parameterizing the far-field time function by the sum of a series of equal-width boxcars. This time function parameterization has the advantage of affording *a priori* control over time function duration and shape which results in fewer inversion parameters. The inverse is completely linear for time function if the source moment tensor or dislocation orientation is known. If time function is known, then the inverse for the moment tensor is completely linear but nonlinear for dislocation parameters. Convergence for joint moment tensor and time function parameters was quick and displayed no adverse starting model dependence for the cases considered. Convergence for dislocation parameters did show adverse characteristics for starting models far from the true model. It is recommended that the grid method and both the moment tensor and dislocation linearized inverse methods be used together to determine source parameters since each technique allows testing of different hypotheses concerning the model and data errors. In particular, dislocation parameters should be found independently from the seismic moment tensor since each model allows a different number of degrees of freedom.

These inverse techniques were applied to near-regional three-component waveform data recorded at the WWSSN station POO from three small, presumably induced, earthquakes associated with the Koyna, India, Reservoir. Occurring on 13 September 1967, 3 months before the main *M*6.4 Koyna earthquake, the locations and radiation patterns of all three were inferred to be virtually identical since waveforms and relative amplitudes recorded at POO and NDI matched even into the low-group velocity coda. The magnitudes of the first two events were estimated to be 4.0 to 4.5 rather than the previously published 5.5 to 6.0. The first event was largest and the magnitude difference between it and the second and third earthquakes was determined to be −0.2 and −0.8, respectively. Results from the grid testing and linearized inverses using event 2 waveforms at POO indicated that source depth was 5 km and that left-lateral movement occurred on a fault striking N20°E ± 5° with a dip of 90° ± 15° and a rake of 0°± 35°. This nodal plane was

chosen as the fault plane on the basis of a fault map constructed from interpretation of LANDSAT images for the Koyna area. Most faults near the reservoir follow NNW to NNE trends and occur in a broad zone paralleling the Western Ghats. The duration of the inferred time function was unusually long at about 3 sec and, with the inferred seismic moment of 9×10^{22} dyne-cm for event 2, suggests a possible stress drop of only 0.05 bar. The orientation and depth found for the second event of 13 September agrees very well with parameters determined from a teleseismic body wave study of the large 10 December 1967, Koyna earthquake, suggesting that these events occurred on the same fault.

ACKNOWLEDGMENTS

This work was stimulated in part by the author's participation in a USGS sponsored workshop on earthquake parameters held in Denver, Colorado, in March 1979. The author is particularly indebted to Paul Richards for useful comments and discussions concerning moment tensors and to David VonSeggern and Roy Greenfield for their critical appraisals of the manuscript. This work was supported by the National Science Foundation under Grant EAR 77-21458 and by the Advanced Research Projects Agency of the Department of Defense and was monitored by the Air Force Office of Scientific Research under Grant AFOSR-78-3528.

REFERENCES

Athavale, R. N. (1975). Induced seepage along a coastal parallel system of faults as a possible cause of the Koyna earthquakes, *Bull. Seism. Soc. Am.* **65,** 183–191.

Brune, J. N. (1970). Tectonic stress and the spectra of seismic shear waves from earthquakes, *J Geophys. Res.* **75,** 4997–5009

Burdick, L. J. and G R. Mellman (1976) Inversion of the body waves from the Borrego Mountain earthquake to the source mechanism, *Bull. Seism. Soc. Am.* **66,** 1485–1500.

Burdick, L. J. and C A. Langston (1977). Modeling crustal structure through the use of converted phases in teleseismic body-wave forms, *Bull. Seism. Soc. Am.* **67,** 677–691

Geller, R. J. (1976). Body force equivalents for stress-drop seismic sources, *Bull. Seism. Soc Am* **66,** 1801–1804.

Gilbert, F. (1970). Excitation of the normal modes of the earth by a point source, *Geophys. J.* **22,** 223–226.

Guha, S. K., P. D. Gosavi, M. M. Varna, S. P. Agarwal, J. G. Padale, and S. C. Mariwadi (1970). *Recent seismic disturbances in the Shivajisagar Lake area of the Koyna Hydroelectric Project, Maharashtra, India*, Central Water and Power Research Station, Poona, India.

Guha, S. K., P D. Gosavi, B. N P. Agarwal, J. G. Padale, and S. C. Mariwadi (1976). Case histories of some artificial crustal disturbances, in *Proceedings of Conference on International Colloquium on Seismic Effects of Reservoir Impounding*, Elsevier, New York.

Gupta, H. K. and J. Coombs (1976). Continued seismic activity at the Koyna reservoir site, India, *Eng. Geol.* **10,** 307–313.

Helmberger, D. V. (1968). The crust-mantle transition in the Bering Sea, *Bull. Seism. Soc. Am.* **58,** 179–214.

Helmberger, D. V. (1974) Generalized ray theory for shear dislocations, *Bull. Seism. Soc. Am.* **64,** 45–64.

Helmberger, D. V. and L R Johnson (1977). Source parameters of moderate size earthquakes and the importance of receiver crustal structure in interpreting observations of local earthquakes, *Bull. Seism Soc Am.* **67,** 301–313.

Jackson, D. D (1979) The use of *a priori* data to resolve non-uniqueness in linear inversion, *Geophys. J.* **57,** 137–157.

Kailasam, L. N., P. R. Pant, S. M. Lahiri, and K. R. M. Simha (1969). Seismic investigations in the Deccan trap areas of Maharashtra and parts of Mysore and Andes Predesh, *Mem. Geol Surv India* **100,** 113–116.

Kanamori, H. and D. L. Anderson (1975). Theoretical basis of some empirical relations in seismology, *Bull. Seism. Soc. Am.* **65,** 1073–1095.

Langston, C. A. (1976). A body wave inversion of the Koyna, India earthquake of December 10, 1967, and some implications for body wave focal mechanisms, *J. Geophys Res.* **81,** 2517–2529.

Langston, C A. (1977). The effect of planar dipping structure on source and receiver responses for constant ray parameter, *Bull. Seism. Soc. Am.* **67,** 1029–1050.

Langston, C. A. (1979). A single-station fault-plane solution method, *Geophys Res. Letters* **6,** 41–44.

Langston, C. A. and D. V. Helmberger (1975). A procedure for modeling shallow dislocation sources, *Geophys. J* **42,** 117–130.

Mendiguren, J. A. (1977). Inversion of surface wave data in source mechanism studies, *J Geophys Res.* **82,** 889–894.

Narain, H. (1973). Crustal structure of the Indian subcontinent, *Tectonophysics* **20,** 249–260.

Narain, H. and H. Gupta (1968). Koyna earthquake, *Nature* **217,** 1138–1139.

Nuttli, O W. (1973). Seismic wave attenuation and magnitude relations for Eastern North America, *J. Geophys. Res.* **78,** 876–885

Peters, D. C and R. S. Crosson (1972). Application of prediction analysis to hypocenter determination using a local array, *Bull. Seism. Soc. Am* **62,** 775–788.

Roy, B. C. (1963). Tectonic map of India (1.2,000,000) Geologic Survey of India, N. K. Gossain & Co., LTD, Calcutta.

Strelitz, R. A. (1978). Moment tensor inversions and source models, *Geophys. J.* **52,** 359–364.

Stump, B. and L. Johnson (1977) The determination of source properties by the linear inversion of seismograms, *Bull. Seism. Soc. Am.* **67,** 1489–1502.

Wiggins, R. A. (1972). The general linear inverse problem implications of surface waves and free oscillations for earth structure, *Rev. Geophys. Space Phys.* **10,** 251–285

Department of Geosciences
Pennsylvania State University
University Park, Pennsylvania 16802

Manuscript received December 27, 1979